# Experimental Measurement of Multiple Hydrate Structure Formation in Binary and Ternary Natural Gas Analogue Systems by Isochoric Equilibrium Methods

# Experimental measurement of multiple hydrate structure formation in binary and ternary natural gas analogue systems by isochoric equilibrium methods

*Morteza Aminnaji[1,3], Ross Anderson[1,2*], Bahman Tohidi[1,2]*

[1]Centre for Gas Hydrate Research, Institute of GeoEnergy Engineering, Heriot-Watt University, Edinburgh EH14 4AS, UK

[2]HydraFACT Ltd., Quantum Court, Heriot-Watt University Research Park, Edinburgh EH14 4AP, UK

[3]Premier Oilfield Group, Aberdeen AB21 0GL, UK

**KEYWORDS:** Gas hydrate formation / dissociation, multiple hydrate structures / phases, equilibrium measurements, isochoric methods, model predictions

**ABSTRACT**

Traditionally, it is commonly assumed that a single gas hydrate (or clathrate hydrate) structure / phase is formed in natural gas systems – e.g., 's-II natural gas (NG) hydrates' or 's-I methane hydrates'– based on that which is understood to be the most thermodynamically stable at incipient phase boundary conditions. This applies with respect to both studies of hydrates in natural sediments, and in the case of hydrocarbon production operations, including in the

testing of low dosage hydrate inhibitors (LDHIs). Here, we present the results of experimental studies of simple propane ($C_3$), binary methane-propane ($C_1$-$C_3$) and ternary methane-ethane-propane ($C_1$-$C_2$-$C_3$) hydrate systems, aimed at investigating phase behaviour at higher subcoolings where significant water conversions to clathrates – and associated gas fractionation – might be expected to result in the formation of more than one hydrate structure. Measurements were made by means of established, reliable, isochoric equilibrium step-heating/cooling approaches. In the single guest propane system, PT (pressure-temperature) conditions follow the gas hydrate phase boundary, in agreement with univariant hydrate + gas + water (H+G+W) equilibrium. By contrast, binary and ternary mixes clearly show PT behaviour consistent with the growth of at least two and four hydrate phases respectively, with these forming sequentially on cooling, and dissociating in the corresponding reverse order upon heating. In-house hydrate model (HydraFLASH®) predictions support experimental observations, pointing to processes being gas fractionation driven; the mixed $C_3$-$C_1$ or $C_3$-$C_2$-$C_1$ s-II type hydrates formed first close to the phase boundary preferentially incorporating the most strongly clathrate cage ($5^{12}6^4$) stabilising propane, making the remaining gas leaner. Once $C_3$ is largely consumed, trends agree with less stable $C_2$-$C_1$ structures (s-II followed by s-I) then growing (where ethane is present), with this, like $C_3$ uptake, making remaining free gas increasingly of almost pure $C_1$. This ultimately drives systems towards final simple, single guest $C_1$ s-I clathrate formation as the well-established univariant phase boundary for this structure is reached. As observed phase behaviour arises because of gas fractionation, it can be expected to occur during hydrate formation in all mixed gas systems of relatively fixed composition (at constant volume or pressure). Findings highlight that care should be taken in application of isochoric methods to multi-component gas systems, given the potential for numerous (rather than just one) clear changes in heating curve slopes as different hydrate

structures form/dissociate. In addition, results show that extending equilibrium steps well into the hydrate region can reveal important information on clathrate phase behaviour with potentially significant implications for issues such as gas production from hydrates in sediments, hydrate technologies for gas capture / separation / storage in the energy industry, and flow assurance in hydrocarbon production operations.

# 1 – Introduction

Gas hydrates are a group of ice-like crystalline inclusion compounds formed through the combination of water and suitably sized 'guest' molecules, typically under low temperature and elevated pressure conditions[1-3]. They are associated with various aspects of current energy production and may well play an increased role in the future. Hydrate plugging is a major flow assurance problem in conventional oil & gas production[1-4], while naturally occurring hydrate deposits in sediments present an abundant source of potentially exploitable lower carbon methane gas[5-7]. Hydrate based technologies could also offer novel means for gas capture, transportation and storage, including for the purposes of $CO_2$ sequestration[8-10].

Various techniques for the measurement of hydrate phase behaviour have been reported in the literature, with these divided into three main categories: isothermal, isobaric, and isochoric[1]. Isothermal techniques involve measurement of pressure changes at constant temperature, with isobaric tests based on determination of thermal behaviour at constant pressure (e.g. differential scanning calorimetry). Probably most popular approach however is isochoric, where the pressure of constant volume systems is measured in response to temperature changes; hydrate formation typically altering the bulk density of phases and so pressure. The hydrate dissociation point can also be determined by visual observation. Generally however, non-visual techniques are more accurate than visual, at least where PT (pressure-temperature) measurement

66 equipment is suitably sensitive, with visual measurements being overly reliant on the ability to
67 see potentially very small fractions of hydrate.

68 Unlike equilibrium dissociation, hydrate nucleation is a stochastic phenomenon, meaning
69 initial hydrate formation PT conditions are generally not repeatable, and dependent on many
70 factors, including mixing efficiency[11], cooling rate, presence of foreign materials[12], fluid
71 composition, water history, and degree of subcooling (ΔT) / temperature. Both the rate of
72 hydrate formation and dissociation can be affected by many factors, including gas composition
73 / cage occupancy[13,14], mass transfer limits[15], presence of liquid hydrocarbons[16,17], presence of
74 surfactants[18,19], and length scales (pore scale or large scale)[20-24]. Metastable hydrate can also
75 exist at some conditions, for example, supercooled water below the freezing point may retard
76 and slow down the dissociation of methane hydrate, i.e., it can exist as a metastable phase[25].
77 Some kinetic hydrate inhibitors, e.g. PVCap (poly-n-vinylcaprolactam), also affect gas hydrate
78 dissociation kinetics and metastable thermodynamic stability[26-31]. Hence, significant literature
79 experimental and numerical modelling work has been undertaken with respect to the accurate
80 measurement of gas hydrate phase behaviour for different systems / conditions[24,32-43].

81 In isochoric approaches, two methods – namely continuous or step heating / cooling – are
82 generally used to change temperature during measurements. In a detailed study, stepwise
83 heating was previously suggested to improve the accuracy of hydrate dissociation data, which
84 could save a significant amount of time[44]. Authors demonstrated that the final hydrate
85 dissociation point (DP) can be accurately determined directly from the intersection of
86 equilibrium cooling / heating curves, as illustrated here in Figure 1. It was also noted how the
87 time requirement for measurements could be reduced by less steps / an increased temperature

88 difference between these, so long as adequate time for equilibrium (as indicated by stable
89 pressure) was given at each step.

90 However, while the step-heating method has distinct advantages, multiple structure formation
91 – and thus multiple potential isochoric system slope changes – could have a significant impact
92 on choice of step heating/cooling patterns and associated interpolation. Anderson et al.[45], Luna-
93 Ortiz et al.[46], Mozaffar et al.[26], and Aminnaji et al.[29] all speculated that more than one hydrate
94 structure could be formed in multi-component gas systems at higher subcoolings in an attempt
95 to explain KHI inhibition patterns. Likewise the formation / co-existence of both s-I and s-II
96 hydrates in methane and methane-ethane gas mixtures has been reported by Schicks and
97 Ripmeester[47] and Ohno et al.[48] respectively.

98 In this work, the results of an experimental study investigating the formation of different
99 hydrate structures in multi-component gas systems using equilibrium isochoric approaches are
100 reported. Experimental data interpretation is supported by model predictions from the in-house
101 commercial HydraFLASH® thermodynamic model. In addition to the importance of findings
102 for understanding hydrate phase behaviour, implications for equilibrium measurements and
103 interpretation are also discussed.

104

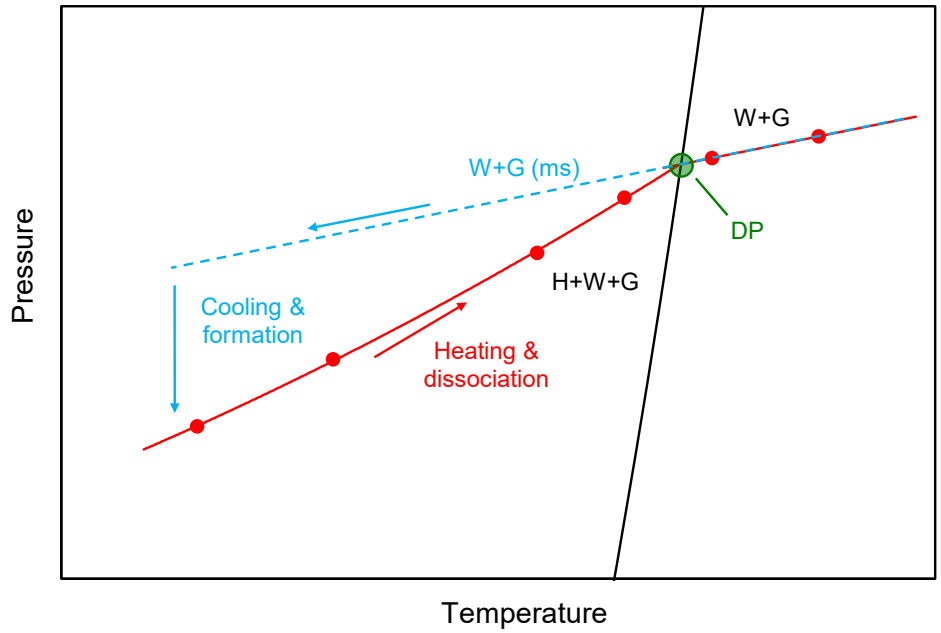


105

106 **Figure 1.** Simplified illustration of the interpolation of cooling and equilibrium step-heating
107 data trends for isochoric gas hydrate dissociation point determination. H = hydrate, W = liquid
108 water, G = free gas / vapour, ms = metastable. The hydrate dissociation point is taken as the
109 intersection of the equilibrium, H+W+ G heating / dissociation curve with the cooling / heating
110 W+G linear trend (metastable inside the hydrate region) as illustrated.

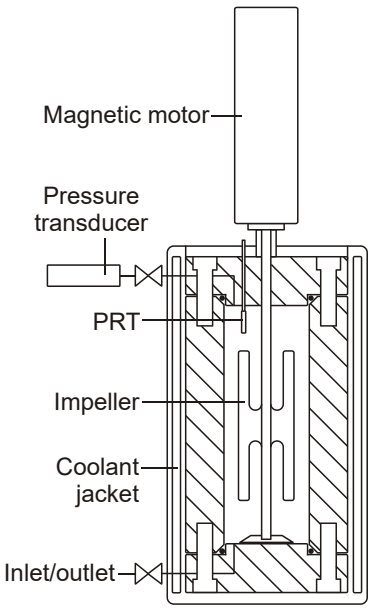


111

112 **Figure 2.** Schematic illustration of the type of high-pressure autoclave cell used in tests.

## 2 – Experimental Methods and Materials

All experiments were carried out using titanium high pressure stirred autoclaves of ~300 ml volume, as shown in Figure 2. An impeller mixing rate of ~500 rpm was typically employed. Cooling jackets were used to control cell temperature by means of circulating glycol-water mixtures from a programmable cryostat unit. Cell temperature and pressure were measured by PRTs (platinum resistance thermometer, calibrated to give an accuracy of ± 0.1 °C) and Druck strain gauges (calibrated using a Budenberg dead weight tester to give an accuracy of ± 0.2 bar) respectively. Distilled water was used in all experiments. In this work, tests were carried out on different gas systems, including pure propane ($C_3$), 98% $C_1$ (methane) + 2% $C_3$, 85% $C_1$ + 12% $C_2$ (ethane) + 3 % $C_3$ (all values in mole%). All gases were supplied by BOC. Propane tests were carried out at 0.7 cell volume fraction water, with mixed gas tests using 0.5 volume fraction water.

In the experiments described here, measurements were carried out as follows. Firstly, systems were cooled rapidly into the hydrate region under mixed conditions to form clathrates. In the propane case, equilibrium step-heating was commenced immediately following this. For the mixed gas tests, systems were instead heated to dissociate most / all of the hydrate present to 'seed' the system with residual hydrates or hydrate 'history', before cells were cooled again at a constant rate of 1 °C/hr to re-grow hydrates, in a similar approach to KHI testing by CGI (crystal growth inhibition) methods[45,26,29]. Following this regrowth, cells were then heated up in steps, with sufficient time given following each temperature step for equilibrium to be achieved (normally on the scale of hours, but sometimes days), as indicated by stable pressure. This step heating was continued until all hydrate had dissociated, as indicated by system PT returning to initial conditions (e.g. cooling line in Figure 1). For the $C_1$+$C_3$ system, further step

cooling measurements were also carried out on a seeded system; this just being the step-heating procedure in reverse, but with nucleation barriers overcome. Although systems were continuously stirred during most measurements, at higher subcoolings in mixed gas systems, the impeller was sometimes blocked by hydrates, which limited mass transfer, meaning equilibrium times were much longer (days to weeks).

Hydrate phase boundaries were predicted using HydraFLASH®, an in-house commercial thermodynamic model by Hydrafact Ltd. (a Heriot-Watt University spin-out company). The sCPA (simplified cubic plus association) equation of state (EoS) option was used. The estimated percentage of water converted to hydrate, as shown in some figures, was calculated using a modified version of that described in Aminnaji et al.[49] from the change in pressure due to hydrate formation; this being assumed as primarily resulting from free gas consumption. Here, gas compressibility ($z$) and water volume expansion to hydrate were additionally accounted for. Values for $z$ as a function of $PT$ were obtained from HydraFLASH, with a hydrate gas hydration ratio of ~1:6 and water volume expansion to hydrate of ~1.25 assumed respectively.

# 3 – Results and discussion

## *3.1. - Single Component Propane System*

Propane is known as a 'simple', single guest hydrate former; it enters and stabilises the large ($5^{12}6^4$) cavity of structure-II, with its molecular diameter too great for the smaller s-I large ($5^{12}6^2$) and s-II/s-I small ($5^{12}$) cages[50]. In this work, isochoric measurements were initially carried out on a propane-water system to demonstrate phase behaviour for single guest gas-water systems where only one hydrate structure is nominally expected.

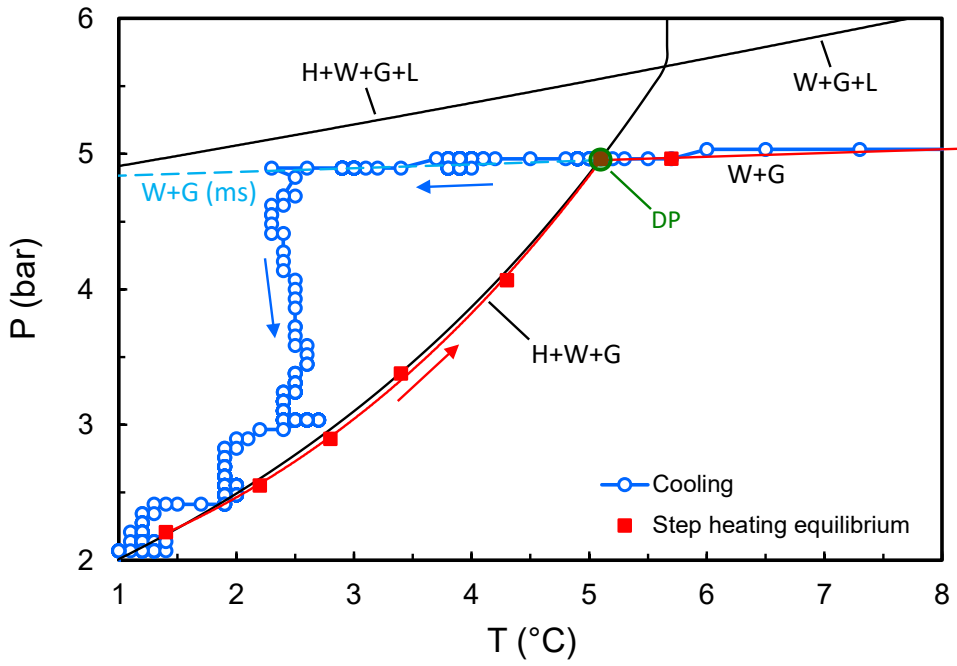


159

160 **Figure 3.** Example pressure / temperature data for tests on the propane + water system,
161 including constant cooling (~1.0 °C / hour) followed by equilibrium step heating, with
162 interpretation for final dissociation point (DP) at incipient hydrate conditions on the (predicted)
163 phase boundary. H = hydrate, W = liquid water, G = gas, L = liquid hydrocarbon phase. Solid
164 black lines are model predictions for the various phase boundaries indicated.

165 **Table 1.** Experimental (exp) step-heating equilibrium pressure-temperature (PT) data points
166 on the H+W+G phase boundary compared HydraFLASH predicted ($P_{pred}$) pressures (at
167 experimental temperatures) for the simple propane-water test system shown in Figure 3. DP =
168 illustrated final dissociation point at incipient hydrate conditions on the phase boundary. AD =
169 absolute deviation from experimental measurement.

| $T_{exp}$ (°C ± 0.2) | $P_{exp}$ (bar ± 0.2) | $P_{pred}$ (bar) | AD (bar) |
|---|---|---|---|
| 1.4 | 2.2 | 2.2 | 0.0 |
| 2.2 | 2.6 | 2.6 | 0.0 |
| 2.8 | 2.9 | 3.0 | +0.1 |
| 3.4 | 3.4 | 3.4 | 0.0 |
| 4.3 | 4.1 | 4.1 | 0.0 |
| $^{(DP)}$5.1 | 5.0 | 4.9 | -0.1 |

Figure 3 shows interpreted cooling/heating pressure-temperature (PT) data for the propane test. Equilibrium step-heating data with HydraFLASH model predicted equilibrium pressures at corresponding temperatures are additionally reported in Table 1. As can be seen, after initial hydrate growth on cooling, as indicated by a sharp reduction in pressure from the linear 'no hydrate' metastable W+G line, subsequent step-heating PT conditions closely follow the propane hydrate univariant phase boundary; the system having 2 components and 3 phases, so one degree of freedom. This continues until all hydrate has dissociated and PT conditions return to the initial W+G cooling line. To accurately determine the final hydrate dissociation point, as per Tohidi et al.[44] and explained in Figure 1, the two curves (heating and cooling) can simply be interpolated, and the intersection taken. Following tests on the single component $C_3$ system, detailed equilibrium isochoric measurements were subsequently carried for two systems of increasing complexity as noted, specifically $C_1$+$C_3$ then $C_1$+$C_2$+$C_3$, as discussed below.

*3.2. - Binary 98% Methane + 2% Propane System*

In contrast to the propane system, as shown in Figure 4, equilibrium step-heating points for the two-component 98 mole% $C_1$ + 2 mole% $C_3$ system clearly show not one, but two heating obvious curve slope changes. The bulk of the measured pressure drop / hydrate formed is associated with a hydrate phase that disappears at DP1. As illustrated in the plot, if heating curve points ahead of this were interpolated with projection forward to the original G+W line as per Figure 1, then an erroneous measurement could result. The reality is of course that a small fraction of a more stable hydrate structure remains above DP1, and this progressively dissociates on approach to the second dissociation point, DP2, which matches well with the model predicted phase boundary for the system.

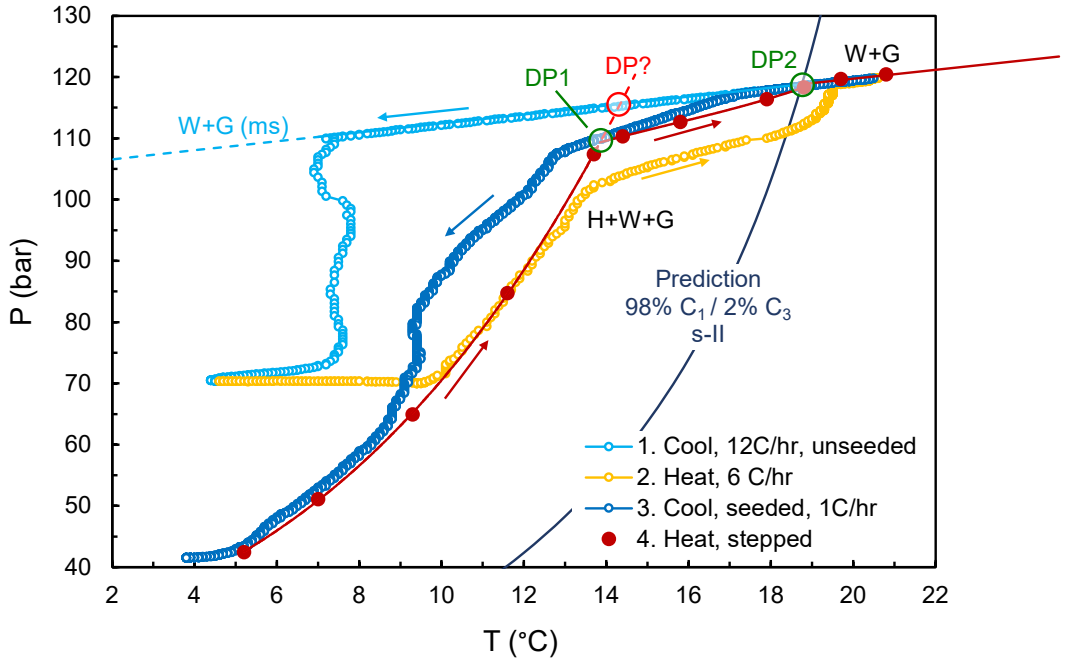


193

194 **Figure 4.** Example PT data for tests on the 98% $C_1$ + 2% $C_3$ gas-water system, including
195 constant cooling (formation) / heating (dissociation) followed by re-cooling then equilibrium
196 step heating trends, with isochoric interpretation of the latter for observed dissociation points
197 (DPs 1 & 2). H = hydrate, W = liquid water, G = gas. 'DP?' illustrates projection of the heating
198 curve for the bulk of the hydrate formed (based on pressure drop / gas consumption) to the
199 metastable (ms) W + G cooling line as per Figure 1, and how this could potentially lead to an
200 erroneous phase boundary measurement if subsequent melting of the smaller remaining
201 fraction of hydrate (to DP2) was accidentally overlooked.

202

203 Clearly, it is difficult to explain observed isochoric phase behaviour without concluding at least
204 two distinct hydrate phases are forming in the $C_1$+$C_3$ system, with these apparently co-existing
205 in equilibrium at higher subcoolings (below DP1). Based on model predictions / experimental
206 data, the clathrates formed in this system are understood to be $C_3$ stabilised mixed guest s-II
207 ($C_3$ in the large cages, $C_1$ in the small) – the most stable phase – and pure s-I methane clathrates

208 at higher subcoolings, as illustrated in Figure 5. Here, to aid in data interpretation / explanation,
209 HydraFLASH model predicted phase boundaries as a function of gas $C_3$ content are
210 superimposed on experimental data. Also shown are subsequent equilibrium step cooling data
211 for the same system; this demonstrating the repeatability of behaviour, with phases
212 growing/dissociating along an identical PT path upon cooling/heating. Equilibrium step-
213 heating data from plots are compared with HydraFLASH model predicted equilibrium
214 pressures at corresponding temperatures in Table 2.

215

216 **Table 2.** Experimental (exp) step-heating equilibrium pressure-temperature (PT) data points
217 compared with HydraFLASH predicted ($P_{pred}$) pressures (where appropriate) for the 98% $C_1$ +
218 2% $C_3$ gas-water system, as show in Figure 4. DP = final dissociation points for the different
219 structures observed, as illustrated. AD = absolute deviation from experimental measurement.

| $T_{exp}$ (°C ± 0.2) | $P_{exp}$ (bar ± 0.2) | $P_{pred}$ (bar) | AD (bar) |
|---|---|---|---|
| 5.2 | 42.5 | 42.4 | -0.1 |
| 7.0 | 51.1 | 50.8 | -0.3 |
| 9.3 | 64.9 | 64.4 | -0.5 |
| 11.6 | 84.7 | 82.7 | -2.0 |
| 13.7 | 107.4 | 105.1 | -2.3 |
| (DP1)13.9 | 109.6 | 107.6 | -2.0 |
| 14.4 | 110.3 | - | - |
| 15.8 | 112.7 | - | - |
| 17.9 | 116.5 | - | - |
| (DP2)18.8 | 118.3 | 122.2 | 3.9 |

220

221

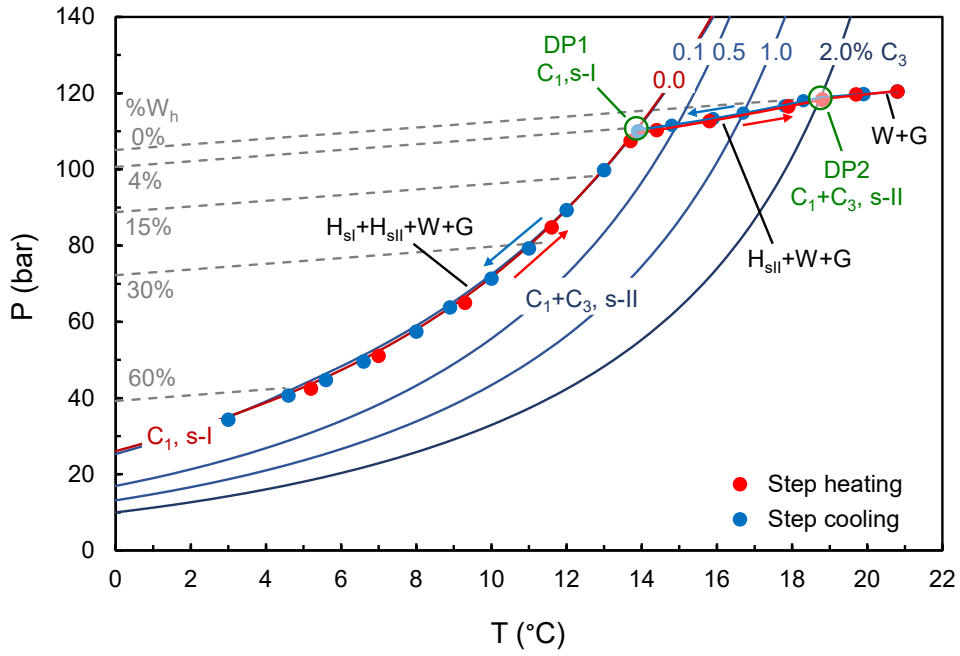


**Figure 5.** Plot of pressure / temperature data for equilibrium step cooling and heating measurements on the 98% $C_1$ / 2% $C_3$ gas + water system. Solid lines are HydraFLASH model predicted phase boundaries for free gas (G) in equilibrium with hydrates (H, with structures indicated, as per text discussions) and free water (W), for the gas compositions shown. DP1 and DP2 are the isochorically determined final dissociation points for the two hydrate structures phase behaviour is consistent with. Dashed grey lines are calculated percent water converted to hydrate $\%W_h$ as a function of pressure drop.

As would be expected, and predicted by the model, mixed propane-methane hydrates (DP2) are notably more stable than simple methane hydrates (DP1), so are those formed at incipient conditions on the phase boundary (for 2% $C_3$). In the presence of a single s-II hydrate, 3 components and 3 phases ($H_{s\text{-}II}$+W+G) yield a system with 2 degrees of freedom / divariant behaviour. As the fraction of propane in the gas is small however, it is insufficient to facilitate conversion of more than a calculated ~4% of water to mixed $C_3$-$C_1$ s-II hydrate. Because of

237 this, the dominant hydrate phase formed in the system must be s-I methane, explaining the two
238 distinct heating / cooling curve slope changes observed.

239 As noted, the isochoric trends observed are driven by gas fractionation; upon cooling and
240 hydrate growth, s-II $C_1$+$C_3$ hydrate forms first, causing the first small pressure drop associated
241 with DP2. This results in a reduction in the $C_3$ concentration in the remaining free gas, as
242 illustrated in model phase boundaries. Along the experimental heating / cooling curve, the
243 hydrate must be in equilibrium with a free gas of the (reducing) $C_3$ fraction shown. As more
244 hydrate grows, so the remnant $C_3$ in the gas continues to decline towards zero, increasingly
245 limiting further s-II growth, gently reducing the heating/cooling curve slope.

246 Eventually, almost all $C_3$ is consumed and remaining free gas becomes almost pure $C_1$. If a
247 methane only hydrate was *not* stable at the PT conditions of interest, then at this point pressure
248 would stop falling (other than due to linear thermal contraction), and no further growth would
249 occur, giving just s-II hydrate, gas and water in equilibrium. However, as shown in Figure 5,
250 system phase behaviour means that gas $C_3$ content in equilibrium with hydrates approaches
251 zero at the pure methane s-I phase boundary. Here, formation of the latter becomes favoured
252 over s-II mixed gas hydrate growth from the now highly dilute $C_3$ in $C_1$. For example, the
253 predicted s-II phase boundary for 0.1% $C_3$ / 99.9% $C_1$ is at a lower temperature (for a given
254 pressure) than that for pure s-I methane clathrates.

255 Therefore, at DP1, the system begins to form simple s-I methane hydrate which co-exists in
256 equilibrium with mixed s-II. The addition of a fourth phase ($H_{s\text{-}I}$+$H_{s\text{-}II}$+W+G) reduces degrees
257 of freedom to 1, and PT conditions start to follow the univariant methane hydrate phase
258 boundary. As more s-I methane hydrate forms, so this would act to re-concentrate $C_3$ in the
259 remaining free gas. However, this in turn will facilitate more mixed s-II growth again as a

260 further small, additional fraction of this becomes stable, keeping the $C_3$ content of the gas free
261 gas very low, and so maintaining univariant conditions. Upon heating, the whole process is
262 reversed, as first s-I methane then mixed s-II hydrates dissociate in turn, resulting in the two
263 distinct dissociation points seen in the $C_1$+$C_3$ system.

264 With respect to measurement techniques, results show that the step-heating method is
265 applicable and accurate in the case of multiple hydrate phases formed over a wide range of
266 temperature. However, as per Figure 4, care should be taken in the frequency of temperature
267 steps and their interpolation. While mixed s-II hydrates are the most stable in the $C_1$-$C_3$ system,
268 the fraction is relatively small, with the bulk of hydrates formed (~90% here) being s-I methane.
269 If the propane content of the initial gas were further reduced, the proportion of s-II hydrates
270 would be likewise, and the 'double dissociation point' could be even less evident in PT
271 relations.

272

273 *3.3. - Ternary 85% Methane + 12% Ethane + 3% Propane System*

274 Following tests on the $C_1$+$C_3$ system, measurements were made on a more complex ternary
275 natural gas analogue, introducing $C_2$. As discussed, binary mixtures of $C_1$+$C_2$ are known to
276 form s-I and/or s-II hydrates, alone or in coexistence, depending on relative guest gas
277 component concentrations and PT conditions[47,48]. Based on results for $C_1$+$C_3$, which show
278 similar behaviour (2 structures), the combined system might be expected to form up to four or
279 more distinct hydrate phases, depending on subcooling / gas fractionation during the hydrate
280 growth process.

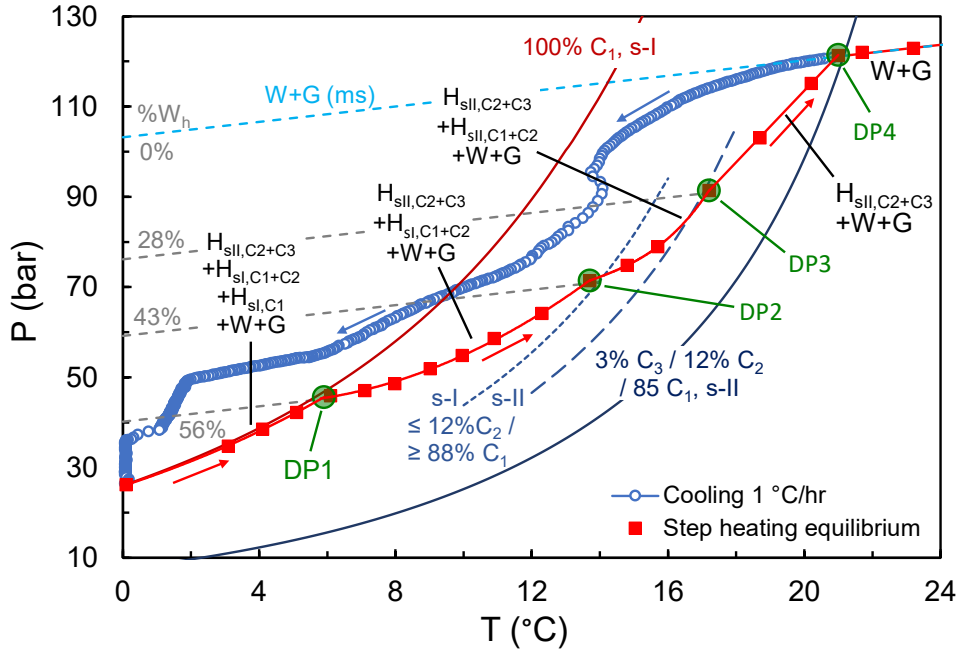


281

282 **Figure 6.** Plot of PT data for constant cooling then equilibrium step heating measurements on
283 the 85% $C_1$ + 12% $C_2$ + 3% $C_3$ + water system. Solid lines are HydraFLASH model predicted
284 equilibrium phase boundaries for free gas (G) in equilibrium with hydrates (H, with suggested
285 structures, including key large cage stabilising guests indicated, as per text discussions) and
286 free water (W), for the gas compositions shown. DP1-4 are the isochorically determined final
287 dissociation points for the four different hydrate phases observed. Dashed grey lines are
288 calculated percent water converted to hydrate $\%W_h$ as a function of pressure drop at the latter.

289

290 Figure 6 shows measured continuous cooling and equilibrium step heating data for the 85% $C_1$
291 + 12% $C_2$ + 3% $C_3$ gas mixture. Step-heating equilibrium PT data points are reported and
292 compared with HydraFLASH predictions (where appropriate) in Table 3. Here, at least four
293 distinct changes in heating curve slope are observed, which is consistent with the sequential
294 dissociation of several different hydrate phases of varying composition and/or structure. Using

295 the phase rule and thermodynamic model predictions, the nature of these phases can be
296 inferred.

297

298 **Table 3.** Experimental (exp) step-heating equilibrium pressure-temperature (PT) data points
299 compared with HydraFLASH predicted ($P_{pred}$) pressures (where appropriate) for the 85% $C_1$ +
300 12% $C_2$ + 3% $C_3$ gas system, as shown in Figure 6. DP = final dissociation points for the
301 different structures observed, as illustrated in the figure. For temperatures of DP1 and below,
302 the remnant gas is assumed as pure $C_1$ for predictions. For DP4, the initial gas composition is
303 used for incipient hydrate conditions. AD = absolute deviation of model prediction from
304 experimental data.

| $T_{exp}$ (°C ± 0.2) | $P_{exp}$ (bar ± 0.2) | $P_{pred}$ (bar) | AD (bar) |
|---|---|---|---|
| 0.1 | 26.2 | 25.5 | -0.7 |
| 3.1 | 34.7 | 34.5 | -0.3 |
| 4.1 | 38.5 | 38.0 | -0.5 |
| 5.1 | 42.2 | 42.0 | -0.2 |
| (DP1)5.9 | 45.6 | 45.5 | -0.1 |
| 6.1 | 45.9 | - | - |
| 7.1 | 47.1 | - | - |
| 8.0 | 48.6 | - | - |
| 9.0 | 51.9 | - | - |
| 10.0 | 54.8 | - | - |
| 10.9 | 58.6 | - | - |
| 12.3 | 64.1 | - | - |
| (DP2)13.7 | 71.4 | - | - |
| 14.8 | 74.8 | - | - |
| 15.7 | 78.9 | - | - |
| (DP3)17.2 | 91.4 | - | - |
| 18.7 | 103.1 | - | - |
| 20.2 | 115.1 | - | - |
| (DP4)21.0 | 121.4 | 117.8 | -3.6 |

305

306

307 At the lowest temperatures / highest water conversions to hydrate, as per the $C_1$+$C_3$ system,
308 heating curve PT points closely follow the established univariant simple methane clathrate
309 phase boundary. This is consistent with the dominant formation/dissociation of pure s-I $C_1$
310 hydrate, which completely disappears at DP1. Again, as per the $C_1$+$C_3$ system, such behaviour
311 would be expected to occur when all ethane and propane had been consumed by hydrates, with
312 the remaining free gas comprising almost pure methane. However, the 4 dissociation points
313 observed at higher temperatures, thus potentially 4 hydrate phases in addition to free water and
314 gas (6 phases and 4 components) present, would imply 0 degrees of freedom, which is
315 inconsistent with the apparent univariant behaviour. The latter requires a single degree of
316 freedom, so just 3 hydrate phases coexisting, for example methane s-I, a mixed methane +
317 ethane phase (s-I or s-II), and the most stable (DP4) methane + propane + ethane s-II.

318 As noted, this univariant-like trend continues until all methane hydrate (it is assumed)
319 dissociates at DP1, and PT conditions leave the established $C_1$ s-I stability region. As
320 temperature is further increased, a new curve is followed from DP1 to DP2, before the next
321 clear slope change occurs. This pattern repeats again to DP3, indicating the progressive
322 dissociation of a further two largely distinct hydrate phases. Given that s-II hydrates stabilised
323 by $C_3$ (and $C_2$) in large cavity ($5^{12}6^4$) are predicted as the most stable (removing $C_3$ from mix
324 depresses the phase boundary as shown), the guest make up of clathrates dissociating at DP2
325 and DP3 would be expected to be primarily comprised of ethane and methane; the addition of
326 $C_2$ increasing hydrate stability compared to $C_1$ alone. As discussed, it is known that ethane can
327 form both stable s-I and s-II hydrates in the presence of methane, entering the large cavity of
328 each ($5^{12}6^2$ and $5^{12}6^4$ respectively), with mixed $C_1$-$C_2$ s-II hydrate being stable to higher
329 temperatures / lower pressures than s-I [50-52]. Therefore, it seems reasonable to propose that DP2
330 and DP3 might be associated with the dissociation of $C_2$ large cavity stabilised hydrates. Model

331 predictions are consistent with this, suggesting the initial melting of $C_2$-$C_1$ mixed s-I
332 ($0.4C_2 \cdot 0.6C_1 \cdot H_2O$) followed by s-II ($0.9C_2 \cdot 1.8C_1 \cdot H_2O$). Approximate phase boundaries for
333 these in Figure 6 were generated by a simple component subtraction approach, i.e. the model
334 was run for s-I and s-II assuming all free gas propane had already been largely consumed by
335 hydrate (in the 28% water conversion associated with DP4) at equilibrium, as shown. Of
336 course, some ethane (and methane) will also have been consumed, and it is not possible to
337 know remnant free gas composition precisely; that would require simultaneous sampling and
338 analysis (an aim of future work). However, the approximations serve to highlight what should
339 occur because of typical gas fractionation, as supported by experimental data.

340 Considering the phase rule, the divariant behaviour observed between $DP_1$ and $DP_3$ suggests
341 more than one degree of freedom in the system. This would imply only a single $C_1$-$C_2$ hydrate
342 phase coexisting with the most stable $C_3$-$C_2$-$C_1$ structure at any given PT, which would agree
343 with the earlier discussed univariant trends below DP1. If this is the case, it might suggest that
344 DP2 could represent a direct solid-solid transition where remaining $C_1$-$C_2$ s-I hydrate changes
345 to s-II before fully dissociating at DP3. Such a phase change would be consistent with literature
346 reports for the binary $C_1$-$C_2$ system, where an s-I ⇌ s-II structure change occurs in response to
347 varying gaseous $C_2$ fraction [50-52].

348 Finally, with propane the most stable hydrate former in this system (large $5^{12}6^4$ cavity of s-II)[50],
349 as would be expected, $C_3$+$C_2$ large cavity stabilised s-II hydrate is the final hydrate phase which
350 dissociates between DP3 and DP4. Model predictions for the initial gas match closely with
351 experimental data for a $C_3$-$C_2$ large cavity stabilised s-II hydrate of composition
352 ~$0.4C_3 \cdot 0.5C_2 \cdot 1.9C_1 \cdot H_2O$ forming/melting at incipient conditions on the phase boundary.

In addition to the above identified phases, although dissociation of $C_1$ s-I was observed at equilibrium here, some studies have previously shown that s-II methane potentially forms as a stable phase at low temperatures and much higher pressures[53-58]. A metastable s-II structure has also been reported at the PT conditions investigated here [47]. Theoretically, methane can enter both the $5^{12}$ and $5^{12}6^4$ cavities of s-II hydrate [50], however, its molecular diameter is insufficient to readily stabilise the large cavity. Therefore, at equilibrium, it typically forms s-I hydrate at the conditions of interest.

With respect to the interpretation of step-heating approaches for hydrate dissociation point measurements, the three-component gas system results again highlight that there may be multiple isochoric slope changes observed in natural gas systems. This means care should be taken in both step temperature interval and interpolation, particularly with respect to the final dissociation point, to ensure accuracy. However, at the same time, extending steps into well into the hydrate region – as opposed to focussing on the region close to the phase boundary – can reveal important information on hydrate behaviour at higher subcoolings. For example, results presented here largely confirm the proposal in previous studies that s-I and other structures can form at high subcoolings, offering a potential failure mechanism for kinetic hydrate inhibitors in natural gas systems [26,29,45,46], e.g. s-II inhibitors failing due to s-I growth.

## 4 – Conclusions

Detailed experimental isochoric equilibrium studies of simple propane, binary methane-propane and ternary methane-ethane-propane systems have been reported. Measurements were made using a reliable step heating/cooling approach. Results for the simple / single gas component propane system show equilibrium PT points to follow the gas hydrate phase boundary, consistent with univariant hydrate + gas + water equilibrium. Only one sharp change

of slope in the heating curve is observed at the final dissociation point, consistent with the dissociation of a single, simple (single guest) hydrate phase. This makes for ready accurate determination of the hydrate phase boundary using established step-heating isochoric approaches.

In contrast to the single-component gas system, studies of the binary and ternary systems over wide temperature ranges / hydrate fractions (up to 60% calculated water conversion) clearly show that the common assumption of a single 'bulk' hydrate phase of one structure – e.g. 's-II natural gas hydrates' – in NG systems is simplistic. Instead, observed phase behaviour is consistent with the formation / dissociation of various hydrate phases / structures which form / dissociate in order of thermodynamic stability. At equilibrium within the hydrate region, it is proposed this process is driven by gas fractionation, which will occur during hydrate growth in both constant volume and variable pressure systems. Model predictions are consistent with this, suggesting the initial melting of s-I $C_1$ hydrates, then mixed $C_2$-$C_1$ structures (s-I followed by s-II) where ethane is present, followed by the most stable s-II $C_3$-$C_1$ or $C_3$-$C_2$-$C_1$ phases.

Findings show that care should be taken in application of step-heating methods to multi-component systems given the potential for numerous clear changes in heating curve slopes as different hydrate structures dissociate. In addition, results demonstrate that extending equilibrium steps well into the hydrate region can reveal important information on phase behaviour with potentially significant implications for issues such as gas production from hydrates in sediments, hydrate technologies for gas capture / separation / storage in the energy industry, and flow assurance in hydrocarbon production operations. For example, findings largely confirm that in addition to the most stable, phase boundary structure (e.g. NG s-II),

398 other structures (e.g. NG s-I) can form at higher subcoolings, offering a potential mechanism
399 for LDHI failure in natural gas systems, as previously speculated for kinetic hydrate inhibitors.

400

## 401 Corresponding Author

402 *Email: ross.anderson@hw.ac.uk

## 403 Acknowledgements

404 M. Aminnaji and R. Anderson contributed equally to this manuscript. B. Tohidi is thanked for
405 his invaluable technical input. This work was funded in whole or in part by Equinor,
406 ChampionX, Total and Engie, whose support is gratefully acknowledged.

## 407 References

408 (1) Sloan Jr, E. Dendy, and Carolyn A. Koh. Clathrate hydrates of natural gases. CRC press,
409 2007.

410 (2) Cochran, S. Hydrate Control and Remediation Best Practices in Deepwater Oil
411 Developments. In *Offshore Technology Conference, OTC 15255. Houston, TX*; 2003.

412 (3) Sloan, E. D.; Koh, C. A.; Sum, A. *Natural Gas Hydrates in Flow Assurance*; Gulf
413 Professional Publishing, 2010.

414 (4) Aminnaji, M.; Tohidi, B.; Burgass, R.; Atilhan, M. Effect of Injected Chemical Density
415 on Hydrate Blockage Removal in Vertical Pipes: Use of MEG/MeOH Mixture to
416 Remove Hydrate Blockage. *J. Nat. Gas Sci. Eng.* **2017**, *45*, 840–847.

417 (5) Sahu, C.; Kumar, R.; Sangwai, J. S. Comprehensive Review on Exploration and Drilling
418 Techniques for Natural Gas Hydrate Reservoirs. *Energy & Fuels* **2020**, *34* (10), 11813–
419 11839.

420 (6) Johnson, A. H. Global Resource Potential of Gas Hydrate--a New Calculation. *Nat. Gas*
421 *Oil* **2011**, *304*, 285–4541.

422 (7) Chong, Z. R.; Yang, S. H. B.; Babu, P.; Linga, P.; Li, X.-S. Review of Natural Gas
423 Hydrates as an Energy Resource: Prospects and Challenges. *Appl. Energy* **2016**, *162*,
424 1633–1652.

425 (8) Rochelle, C. A.; Camps, A. P.; Long, D.; Milodowski, A.; Bateman, K.; Gunn, D.;

426 Jackson, P.; Lovell, M. A.; Rees, J. Can CO2 Hydrate Assist in the Underground Storage
427 of Carbon Dioxide? *Geol. Soc. London, Spec. Publ.* **2009**, *319* (1), 171–183.

428 (9) Tohidi, B.; Yang, J.; Salehabadi, M.; Anderson, R.; Chapoy, A. CO2 Hydrates Could
429 Provide Secondary Safety Factor in Subsurface Sequestration of CO2. *Environ. Sci. &*
430 *Technol.* **2010**, *44* (4), 1509–1514.

431 (10) Hassanpouryouzband, A.; Yang, J.; Tohidi, B.; Chuvilin, E.; Istomin, V.; Bukhanov, B.;
432 Cheremisin, A. Insights into CO2 Capture by Flue Gas Hydrate Formation: Gas
433 Composition Evolution in Systems Containing Gas Hydrates and Gas Mixtures at Stable
434 Pressures. *ACS Sustain. Chem. & Eng.* **2018**, *6* (5), 5732–5736.

435 (11) Qureshi, M. F.; Atilhan, M.; Altamash, T.; Aparicio, S.; Aminnaji, M.; Tohidi, B. High-
436 Pressure Gas Hydrate Autoclave Hydraulic Experiments and Scale-up Modeling on the
437 Effect of Stirring RPM Effect. *J. Nat. Gas Sci. Eng.* **2017**, *38*, 50–58.

438 (12) Chong, Z. R.; Chan, A. H. M.; Babu, P.; Yang, M.; Linga, P. Effect of NaCl on Methane
439 Hydrate Formation and Dissociation in Porous Media. *J. Nat. Gas Sci. Eng.* **2015**, *27*,
440 178–189.

441 (13) Sun, Z.; Wang, H.; Yao, J.; Sun, Z.; Bongole, K.; Zhu, X.; Liu, L.; Wang, J. Effect of
442 Cage-Specific Occupancy on the Dissociation Rate of a Three-Phase Coexistence
443 Methane Hydrate System: A Molecular Dynamics Simulation Study. *J. Nat. Gas Sci.*
444 *Eng.* **2018**, *55*, 235–242.

445 (14) Smith, C.; Barifcani, A.; Pack, D. Gas Hydrate Formation and Dissociation Numerical
446 Modelling with Nitrogen and Carbon Dioxide. *J. Nat. Gas Sci. Eng.* **2015**, *27*, 1118–
447 1128.

448 (15) Feyzi, V.; Mohebbi, V. Experimental Study and Modeling of the Kinetics of Carbon-
449 Dioxide Hydrate Formation and Dissociation: A Mass Transfer Limited Kinetic
450 Approach. *J. Nat. Gas Sci. Eng.* **2020**, *77*, 103273.

451 (16) Song, G.; Li, Y.; Wang, W.; Jiang, K.; Shi, Z.; Ye, X.; Zhao, P. Experimental Study of
452 Hydrate Dissociation in Oil-Dominated Systems Using a High-Pressure Visual Cell. *J.*
453 *Nat. Gas Sci. Eng.* **2017**, *45*, 26–37.

454 (17) Kakati, H.; Kar, S.; Mandal, A.; Laik, S. Methane Hydrate Formation and Dissociation
455 in Oil-in-Water Emulsion. *Energy & Fuels* **2014**, *28* (7), 4440–4446.

456 (18) Karaaslan, U.; Parlaktuna, M. On the Dissociation of Natural Gas Hydrates from
457 Surfactant Solutions. *Energy & fuels* **2001**, *15* (1), 241–246.

458 (19) Gudala, M.; Govindarajan, S. K.; Mandal, A. Chemical Affinity Modeling of Methane
459 Hydrate Formation and Dissociation in the Presence of Surfactants. *Energy & Fuels*
460 **2019**, *34* (1), 319–331.

461 (20) Park, T.; Lee, J. Y.; Kwon, T.-H. Effect of Pore Size Distribution on Dissociation
462 Temperature Depression and Phase Boundary Shift of Gas Hydrate in Various Fine-
463 Grained Sediments. *Energy & Fuels* **2018**, *32* (4), 5321–5330.

464 (21) Tsimpanogiannis, I. N. Study of the Critical Gas Saturation during Methane Hydrate
465 Dissociation at the Single-Pore Scale: Analytical Solutions for Large Pores. *J. Nat. Gas*

*Sci. Eng.* **2020**, *83*, 103577.

(22) Pandey, J. S.; Almenningen, S.; von Solms, N.; Ersland, G. Pore-Scale Visualization of CH4 Gas Hydrate Dissociation under Permafrost Conditions. *Energy & Fuels* **2021**, *35* (2), 1178–1196.

(23) Rojas Zuniga, A.; Li, M.; Aman, Z. M.; Stanwix, P. L.; May, E. F.; Johns, M. L. NMR-Compatible Sample Cell for Gas Hydrate Studies in Porous Media. *Energy & Fuels* **2020**, *34* (10), 12388–12398.

(24) Sun, Y.-H.; Su, K.; Li, S.-L.; Carroll, J. J.; Zhu, Y.-H. Experimental Investigation into the Dissociation Behavior of CH4--C2H6--C3H8 Hydrates in Sandy Sediments by Depressurization. *Energy & Fuels* **2018**, *32* (1), 204–213.

(25) Sun, R.; Fan, Z.; Yang, M.; Pang, W.; Li, Y.; Song, Y. Experimental Investigation into the Dissociation of Methane Hydrate near Ice-Freezing Point Induced by Depressurization and the Concomitant Metastable Phases. *J. Nat. Gas Sci. Eng.* **2019**, *65*, 125–134.

(26) Mozaffar, H.; Anderson, R.; Tohidi, B. Reliable and Repeatable Evaluation of Kinetic Hydrate Inhibitors Using a Method Based on Crystal Growth Inhibition. *Energy & Fuels* **2016**, *30* (12), 10055–10063.

(27) Gulbrandsen, A. C.; Svartås, T. M. Effects of PVCap on Gas Hydrate Dissociation Kinetics and the Thermodynamic Stability of the Hydrates. *Energy & Fuels* **2017**, *31* (9), 9863–9873.

(28) Altamash, T.; Qureshi, M. F.; Aparicio, S.; Aminnaji, M.; Tohidi, B.; Atilhan, M. Gas Hydrates Inhibition via Combined Biomolecules and Synergistic Materials at Wide Process Conditions. *J. Nat. Gas Sci. Eng.* **2017**, *46*, 873–883.

(29) Aminnaji, M.; Anderson, R.; Tohidi, B. Anomalous KHI-Induced Dissociation of Gas Hydrates inside the Hydrate Stability Zone: Experimental Observations & Potential Mechanisms. *J. Pet. Sci. Eng.* **2019**, *178*, 1044–1050.

(30) Gulbrandsen, A. C.; Svartaas, T. M. Influence on Hydrate Dissociation for Methane Hydrates Formed in the Presence of PolyVinylCaprolactam versus PolyVinylCaprolactam+ Butyl Glycol Ether. *Energy & Fuels* **2017**, *31* (6), 6352–6357.

(31) Mardani, M.; Azimi, A.; Javanmardi, J.; Mohammadi, A. H. Effect of EMIM-BF4 Ionic Liquid on Dissociation Temperature of Methane Hydrate in the Presence of PVCap: Experimental and Modeling Studies. *Energy & Fuels* **2018**, *33* (1), 50–57.

(32) Dharmawardhana, P. B.; Parrish, W. R.; Sloan, E. D. Experimental Thermodynamic Parameters for the Prediction of Natural Gas Hydrate Dissociation Conditions. *Ind. & Eng. Chem. Fundam.* **1980**, *19* (4), 410–414.

(33) Avlonitis, D. The Determination of Kihara Potential Parameters from Gas Hydrate Data. *Chem. Eng. Sci.* **1994**, *49* (8), 1161–1173.

(34) Circone, S.; Stern, L. A.; Kirby, S. H. The Role of Water in Gas Hydrate Dissociation. *J. Phys. Chem. B* **2004**, *108* (18), 5747–5755.

(35) Li, J.; Liang, D.; Guo, K.; Wang, R.; Fan, S. Formation and Dissociation of HFC134a Gas Hydrate in Nano-Copper Suspension. *Energy Convers. Manag.* **2006**, *47* (2), 201–210.

(36) Atik, Z.; Windmeier, C.; Oellrich, L. R. Experimental Gas Hydrate Dissociation Pressures for Pure Methane in Aqueous Solutions of MgCl2 and CaCl2 and for a (Methane+ Ethane) Gas Mixture in an Aqueous Solution of (NaCl+ MgCl2). *J. Chem. & Eng. data* **2006**, *51* (5), 1862–1867.

(37) Kwon, T.-H.; Cho, G.-C.; Santamarina, J. C. Gas Hydrate Dissociation in Sediments: Pressure-Temperature Evolution. *Geochemistry, Geophys. Geosystems* **2008**, *9* (3).

(38) Mohammadi, A. H.; Richon, D. Gas Hydrate Phase Equilibrium in the Presence of Ethylene Glycol or Methanol Aqueous Solution. *Ind. & Eng. Chem. Res.* **2010**, *49* (18), 8865–8869.

(39) Javanmardi, J.; Babaee, S.; Eslamimanesh, A.; Mohammadi, A. H. Experimental Measurements and Predictions of Gas Hydrate Dissociation Conditions in the Presence of Methanol and Ethane-1, 2-Diol Aqueous Solutions. *J. Chem. & Eng. Data* **2012**, *57* (5), 1474–1479.

(40) Bhade, P.; Phirani, J. Effect of Geological Layers on Hydrate Dissociation in Natural Gas Hydrate Reservoirs. *J. Nat. Gas Sci. Eng.* **2015**, *26*, 1549–1560.

(41) Sadeq, D.; Iglauer, S.; Lebedev, M.; Smith, C.; Barifcani, A. Experimental Determination of Hydrate Phase Equilibrium for Different Gas Mixtures Containing Methane, Carbon Dioxide and Nitrogen with Motor Current Measurements. *J. Nat. Gas Sci. Eng.* **2017**, *38*, 59–73.

(42) Hu, Y.; Lee, B. R.; Sum, A. K. Phase Equilibrium Data of Methane Hydrates in Mixed Brine Solutions. *J. Nat. Gas Sci. Eng.* **2017**, *46*, 750–755.

(43) Truong-Lam, H. S.; Seo, S.; Kim, S.; Seo, Y.; Lee, J. D. In Situ Raman Study of the Formation and Dissociation Kinetics of Methane and Methane/Propane Hydrates. *Energy & Fuels* **2020**, *34* (5), 6288–6297.

(44) Tohidi, B.; Burgass, R. W.; Danesh, A.; Østergaard, K. K.; Todd, A. C. Improving the Accuracy of Gas Hydrate Dissociation Point Measurements. *Ann. N. Y. Acad. Sci.* **2000**, *912* (1), 924–931.

(45) Anderson, R.; Mozaffar, H.; Tohidi, B. Development of a Crystal Growth Inhibition Based Method for the Evaluation of Kinetic Hydrate Inhibitors. In *Proceedings of the 7th International Conference on Gas Hydrates*; 2011; pp 17–21.

(46) Luna-Ortiz, E.; Healey, M.; Anderson, R.; Sørhaug, E. Crystal Growth Inhibition Studies for the Qualification of a Kinetic Hydrate Inhibitor under Flowing and Shut-In Conditions. *Energy & Fuels* **2014**, *28* (5), 2902–2913.

(47) Schicks, J. M.; Ripmeester, J. A. The Coexistence of Two Different Methane Hydrate Phases under Moderate Pressure and Temperature Conditions: Kinetic versus Thermodynamic Products. *Angew. Chemie Int. Ed.* **2004**, *43* (25), 3310–3313.

(48) Ohno, H.; Strobel, T. A.; Dec, S. F.; Sloan Jr, E. D.; Koh, C. A. Raman Studies of

545 Methane- Ethane Hydrate Metastability. *J. Phys. Chem. A* **2009**, *113* (9), 1711–1716.

546 (49) Aminnaji, M.; Tohidi, B.; Burgass, R.; Atilhan, M. Gas Hydrate Blockage Removal
547 Using Chemical Injection in Vertical Pipes. *J. Nat. Gas Sci. Eng.* **2017**.

548 (50) Sloan, E. D. Fundamental Principles and Applications of Natural Gas Hydrates. *Nature*
549 **2003**, *426* (6964), 353–363.

550 (51) Takeya, S.; Kamata, Y.; Uchida, T.; Nagao, J.; Ebinuma, T.; Narita, H.; Hori, A.;
551 Hondoh, T. Coexistence of Structure I and II Hydrates Formed from a Mixture of
552 Methane and Ethane Gases. *Can. J. Phys.* **2003**, *81* (1–2), 479–484.

553 (52) Subramanian, S.; Kini, R. A.; Dec, S. F.; Sloan, E. D. Evidence of Structure II Hydrate
554 Formation from Methane+ Ethane Mixtures. *Chem. Eng. Sci.* **2000**, *55* (11), 1981–1999.

555 (53) Hirai, H.; Kondo, T.; Hasegawa, M.; Yagi, T.; Yamamoto, Y.; Komai, T.; Nagashima,
556 K.; Sakashita, M.; Fujihisa, H.; Aoki, K. Methane Hydrate Behavior under High
557 Pressure. *J. Phys. Chem. B* **2000**, *104* (7), 1429–1433.

558 (54) Hirai, H.; Uchihara, Y.; Fujihisa, H.; Sakashita, M.; Katoh, E.; Aoki, K.; Nagashima,
559 K.; Yamamoto, Y.; Yagi, T. High-Pressure Structures of Methane Hydrate Observed up
560 to 8 GPa at Room Temperature. *J. Chem. Phys.* **2001**, *115* (15), 7066–7070.

561 (55) Chou, I.-M.; Sharma, A.; Burruss, R. C.; Shu, J.; Mao, H.; Hemley, R. J.; Goncharov,
562 A. F.; Stern, L. A.; Kirby, S. H. Transformations in Methane Hydrates. *Proc. Natl. Acad.*
563 *Sci.* **2000**, *97* (25), 13484–13487.

564 (56) Loveday, J. S.; Nelmes, R. J.; Guthrie, M.; Belmonte, S. A.; Allan, D. R.; Klug, D. D.;
565 Tse, J. S.; Handa, Y. P. Stable Methane Hydrate above 2 GPa and the Source of Titan's
566 Atmospheric Methane. *Nature* **2001**, *410* (6829), 661–663.

567 (57) Shimizu, H.; Kumazaki, T.; Kume, T.; Sasaki, S. In Situ Observations of High-Pressure
568 Phase Transformations in a Synthetic Methane Hydrate. *J. Phys. Chem. B* **2002**, *106* (1),
569 30–33.

570 (58) Stoporev, A. S.; Ogienko, A. G.; Sizikov, A. A.; Semenov, A. P.; Kopitsyn, D. S.;
571 Vinokurov, V. A.; Svarovskaya, L. I.; Lubov'K, A.; Manakov, A. Y. Unexpected
572 Formation of SII Methane Hydrate in Some Water-in-Oil Emulsions: Different Reasons
573 for the Same Phenomenon. *J. Nat. Gas Sci. Eng.* **2018**, *60*, 284–293.

574